Density functional theory study of the mechanism of Li diffusion in rutile RuO2

Jongboo Jung, Maenghyo Cho, and Min Zhou

Citation: AIP Advances **4**, 017104 (2014); doi: 10.1063/1.4861583
View online: http://dx.doi.org/10.1063/1.4861583
View Table of Contents: http://scitation.aip.org/content/aip/journal/adva/4/1?ver=pdfcov
Published by the AIP Publishing

AIP ADVANCES **4**, 017104 (2014)

Density functional theory study of the mechanism of Li diffusion in rutile RuO_2

Jongboo Jung,[1] Maenghyo Cho,[1] and Min Zhou[1,2,a]
[1]*WCU Program on Multiscale Mechanical Design, School of Mechanical and Aerospace Engineering, Seoul National University, Seoul 151-742, Republic of Korea*
[2]*George W. Woodruff School of Mechanical Engineering, School of Materials Science and Engineering, Georgia Institute of Technology, Atlanta, Georgia 30332-0405, USA*

(Received 11 August 2013; accepted 16 December 2013; published online 6 January 2014)

First-principle calculations are carried out to study the diffusion of Li ions in rutile structure RuO_2, a material for positive electrodes in rechargeable Li ion batteries. The calculations focus on migration pathways and energy barriers for diffusion in Li-poor and Li-rich phases using the Nudged Elastic Band Method. Diffusion coefficients estimated based on calculated energy barriers are in good agreement with experimental values reported in the literature. The results confirm the anisotropic nature of diffusion of Li ions in one-dimensional c channels along the [001] crystalline direction of rutile RuO_2 and show that Li diffusion in the Li-poor phase is faster than in the Li-rich phase. The findings of fast Li diffusion and feasible Li insertion at low temperatures in the host rutile RuO_2 suggest this material is a good ionic conductor for Li transport. The finding also suggests possible means for enhancing the performance of RuO_2-based electrode materials. [http://dx.doi.org/10.1063/1.4861583]

I. INTRODUCTION

As demand for lithium ion batteries increases, extensive experimental and theoretical research on promising electrode materials has been conducted. Ideal electrodes should have flexible structures, large reversible capacities, low cost, high and consistent voltages, structural integrity, non-toxicity, ionic bonding, and good electronic conductivity. Transition metal oxides possess many of these attributes and are therefore promising candidates for high-performance electrode materials. Lithium cobalt oxide ($LiCoO_2$) is the most commercialized cathode material and $LiFePO_4$ has received attention as a next generation material. RuO_2, one of the transition metal oxides having the rutile structure, has been recently attracting interest for its unusual characteristics in lithium insertion. In particular, it has an extremely high total capacity of 1130 mAg^{-1} and high first-cycle Coulombic efficiency of above 98%.[1]

Upon lithiation, rutile RuO_2 is topotactically transformed into orthorhombic $LiRuO_2$. During the charge or discharge process in the electrodes, a tetragonal intermediate buffer phase exists between RuO_2 and $LiRuO_2$ to relax stresses due to lattice mismatch.[2] This homogeneous transformation process leads to a maximum lithium storage capacity of 200 mAh/g in the first discharge.[1] This process can be further followed by the heterogeneous formation of Ru/Li_2O with interfacial accommodation of Li^+ ions, which permits the storage of 5.6 Li^+ ions per unit RuO_2.[1,3] With its unique, favorable combination of high capacity and high Coulombic efficiency, RuO_2 is a theoretically and practically attractive lithium storage material. Despite concerns about capacity fading after the first few cycles,[1] efforts to maximize the advantages of this material in practice have continued through combination with carbon, which results in RuO_2/C self-wound nanomembranes (SWNMs),[4] use

[a]To whom correspondence should be addressed, Email: min.zhou@gatech.edu

as interconnect with $FePO_4$,[5] and formation of nanocomposites with amorphous V_2O_5 aerogels.[6] Moreover, coating on other materials shows that a RuO_2 surface layer facilitates fast electron transfer as well as fast Li^+ ion diffusion.[7] Experimental studies on the kinetic characteristics of Li ions in this material have been reported,[8–10] yet to the best of our knowledge, no theoretical investigation involving quantitative analyses of the diffusion process at the atomic level has been carried out. To better design electrode materials with enhanced capacity and charge/discharge speeds, it is important to systematically identify and quantify the effective pathways for Li diffusion and the associated diffusivities. Understanding the nature of Li diffusion and quantifying the ionic conductivity are one key to the design of materials with improved capacities.

In this research, we conduct a first-principle investigation into the diffusion of Li in rutile-structured RuO_2 in order to understand the nature of Li diffusion. Under the assumption of high electronic conductivity, which is the case for RuO_2,[4,11] the intrinsic ionic diffusivity and Li diffusion pathways can be determined by examining the activation barriers along Li hopping paths. Potential migration pathways are analyzed in both the Li-rich and Li-poor phases. The calculations reveal the anisotropic one-dimensional pathways in RuO_2 and allow the diffusivity to be quantified via the transition state theory with accurately calculated effective phonon frequencies. A comparison is made with the diffusional behavior of Li in rutile TiO_2 which has the same structure as RuO_2. The result shows that rutile RuO_2 is a good candidate cathode material in terms of stable Li intercalation at low temperatures (an attribute not seen in TiO_2) and in terms of high Li diffusivity. Different Li diffusional behaviors are revealed for different extreme phases and the insight can qualitatively explain aspects of diffusional behaviors observed in experiments.

II. COMPUTATIONAL METHODS

The first-principle calculations carried out are based on the density functional theory (DFT) and use the Vienna *Ab-initio* Simulation Package (VASP)[12] with the projector augmented-wave (PAW)[13,14] approach and generalized gradient approximation (GGA) exchange correlation functional of Perdew-Wang 1991.[15] The pseudopotential deals with all three electrons of Li (Li_sv) with the 1s shell being treated as valence states**,** and the standard potentials of Ru and O are used. A single plane wave energy cut-off of 800 eV is used and the first Brillouin zone is sampled for k-space integration using a Monkhorst-Pack grid. A k-point mesh of $5 \times 5 \times 5$ is used for all calculations.

The nudged elastic band method (NEB)[16,17] implemented in VASP is used to determine the diffusion pathways and migration energy barriers. The detailed calculation procedure is as follows. The structures of RuO_2 and $LiRuO_2$ are optimized via full relaxation of lattice parameters as well as atomic positions by calculating the Hellmann-Feynman force until the residual forces acting on the atoms are smaller than 0.03 eV/Å. The NEB calculations are performed in supercells consisting of $2a \times 2b \times 2c$ unit cells containing 16 formula units to reduce interactions between images due to the periodic boundary conditions used. Structural parameters of perfect RuO_2 or $LiRuO_2$ are used for models of the Li-poor phase and the Li-rich phase, respectively. One Li vacancy is introduced in the $LiRuO_2$ structure for the Li-rich phase which is composed of 63 atoms ($Li_{15}Ru_{16}O_{32}$), whereas a Li is added to the RuO_2 structure for the Li-poor phase which is composed of 49 atoms ($Li_1Ru_{16}O_{32}$). Under the assumption that the local motion of a Li ion does not perturb the shape of the overall material structure, internal coordinates are fully relaxed while lattice constants and volumes are kept fixed at those of perfect crystalline structures of $LiRuO_2$ and RuO_2 for the Li-rich phase and Li-poor phase, respectively. End positions are created as equivalent of initial positions at the nearest neighbor corresponding to the local energy minima. Seven images are then linearly interpolated between the initial and end positions along Li migration pathways. All atoms are relaxed until the residual forces acting on each atom are smaller than 0.03 eV/Å. In the NEB, all replicated images are connected with neighboring images and can move only in the direction perpendicular to the hypertangent between two neighboring images, maintaining equal distances between the neighbors. For the migration paths with the lowest energy barriers in both phases, NEB calculations with 15 interpolated images are performed to confirm the existence of a unique saddle point along the diffusion path. The calculations identify the minimum energy pathways of lithium ions hopping in the structures.

TABLE I. Structural parameters for RuO_2 and $LiRuO_2$. Optimized lattice parameters, volume, and Wyckoff positions are listed and compared with available experimental results.

	$LiRuO_2$	$LiRuO_2$-exp[2]	RuO_2	RuO_2-exp[2]
Space group	*Pnnm*		$P4_{2/mnm}$	
a (Å)	5.154	5.055	4.542	4.491
b (Å)	5.031	4.954	4.542	4.491
c (Å)	2.785	2.774	3.141	3.105
V (Å^3)	72.22	69.47	64.81	62.63
	Wyckoff Positions			
Li	2c (0, 1/2, 0) or 2d (1/2, 0, 0)			
Ru	2a (0, 0, 0)		2a (0, 0, 0)	
O	4g (x, y, 0)		4f (x, x, 0)	
	x = 0.248	x = 0.26	x = 0.306	x = 0.31
	y = 0.329	y = 0.33		

III. RESULTS AND DISCUSSION

A. Structure

The perfect structures of RuO_2 and $LiRuO_2$ without defect are optimized via full relaxation. Optimized lattice parameters are listed and compared with experimental values reported in the literature in Table I. Our results for relaxed lattice parameters and atomic positions show good agreement with experimental values and previous DFT calculations.[2,18,19] The calculated lattice constant values are slightly larger than the experimental values, due to the GGA approximation which commonly leads to overestimate of lattice constants.

The crystalline structures of RuO_2 and $LiRuO_2$ are shown in Figure 1. The rutile structure (space group 136, $P4_{2/mnm}$) has an hcp oxygen lattice in which the metal ions and octahedra form edge sharing chains in the [001] direction along the *c*-axis.[11,19] The chains are cross-linked by sharing corners to form an equal number of identical vacant channels. The incorporation of Li ions in the rutile host is in these channels, at octahedral sites of 2(c) or 2(d).[2] Upon lithiation, the lengths of the *a* axis of a square base increase from 4.491 Å to 5.055 Å and 4.954 Å, converting the square base to a rectangular base. Meanwhile the length of the *c* axis decreases due to strong metal-metal bonding, resulting in a transformation of the lattice structure from tetragonal ($a = b \neq c$) to orthorhombic ($a \neq b \neq c$) with the change of the *c*/*a* ratio from 0.691 to 0.549. The structure after lithiation has the space group of 58 (*Pnnm*).[20] A Bader charge analysis is conducted to explore the nature of bonding in the material.[21,22] In this method, the Bader volume is defined as the space enclosed by the surface perpendicular to the electron charge density minimum and the atomic charge can be taken as the integration of the charge density within the region.

The average charges for each atomic species in $LiRuO_2$, RuO_2, Li-rich, and Li-poor phases are listed in Table II. The charge of Li in the fully discharged state, $LiRuO_2$, is $+0.853e$ which shows a strong ionic characteristic in the host material. Charges of Li atoms in the Li-rich phase are in the range from $+0.852e$ to $+0.856e$ and the charge of the Li atom near the vacancy introduced is $+0.856e$. When the migrating atom is at a saddle point, its charge is $+0.851e$ which is about the same as the charge at the initial point. This indicates that Li is kept ionized in the diffusion process. In the Li-poor phase, the Li atom has a charge of $+0.815e$ which suggests the atom is slightly less oxidized. This indicates a slightly more covalent nature of conditions for the Li ion in this phase compared with the Li-rich or fully charged state. This finding is echoed by the Li-O shorter bond length of 1.795 Å in contrast to the length of 2.068 Å in the Li-rich phase.

The charge for Ru is $+1.247e$ in $LiRuO_2$ and $+1.630e$ in RuO_2, and the charge for O is $-1.050e$ in $LiRuO_2$ and $-0.815e$ in RuO_2. This is in contrast to the formal ionization states, in which all bonds between atoms are assumed to be ionic, of Ru^{4+} in RuO_2 and Ru^{3+} in $LiRuO_2$. Similarly, the calculated charges of O atoms deviate from the formal charge of -2 in both $LiRuO_2$ and RuO_2 The

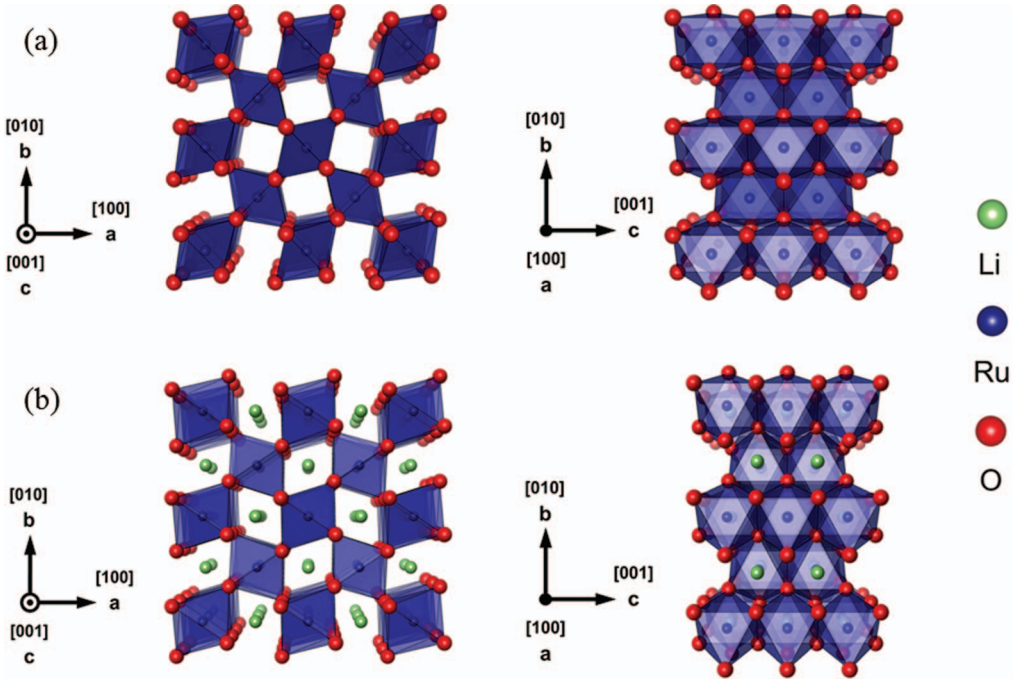

FIG. 1. Crystalline structures of (a) RuO_2 and (b) $LiRuO_2$. Li, Ru and O atoms are represented as green, blue, and red spheres, respectively. RuO_6 are marked by blue octahedrons. Graphical representations are generated using the VESTA visualization software program.[16]

TABLE II. Bader charges of each atomic species in $LiRuO_2$ and RuO_2 (overall average).

	Bader Charge			
Atom	$LiRuO_2$	RuO_2	Li-rich	Li-poor
Li	+0.853		+0.853	+0.815
Ru	+1.247	+1.630	+1.266	+1.609
O	− 1.050	− 0.815	− 1.033	− 0.830

charges of Ru and O in the Li-poor and Li-rich phases are similar to those in RuO_2 and $LiRuO_2$, respectively. These show a partial covalent characteristic of the RuO_6 polyanions in the compounds.

B. Migration energy barriers in Li-rich phase

It is believed that Li diffuses in one channel along the *c* direction in the rutile structure[20] and *ab initio* studies confirmed that it is indeed the case for the Li diffusion in rutile TiO_2.[23,24] However, no theoretical calculation has been carried out for the migration barrier in RuO_2. Furthermore, no quantitative comparison has been made with other possible pathways. In this study, we consider different plausible pathways for Li migration and evaluate their migration barriers, accounting for the migration distances between Li sites. Two extreme Li-intercalated states of the host structures are taken into account due to the fact that the electrodes consist of hetero-junctions between distinct phases. During the charge-discharge process, the proportion of each of the $LiRuO_2$, RuO_2, and the intermediate buffer phases changes with the movement of the phase boundaries separating the phases.[2] Therefore, the diffusion process of Li mainly occurs in these extreme phases. For each of the Li-rich and Li-poor phases, three potential pathways are considered based on the specific geometry. Figure 2 shows the potential pathways for Li diffusion in the host. These pathways correspond to movement along the *b*-axis in the [010] direction directly through the edge-sharing RuO_6 octahedrons (Path A), movement to the nearest neighbor in the next diagonal channel in the

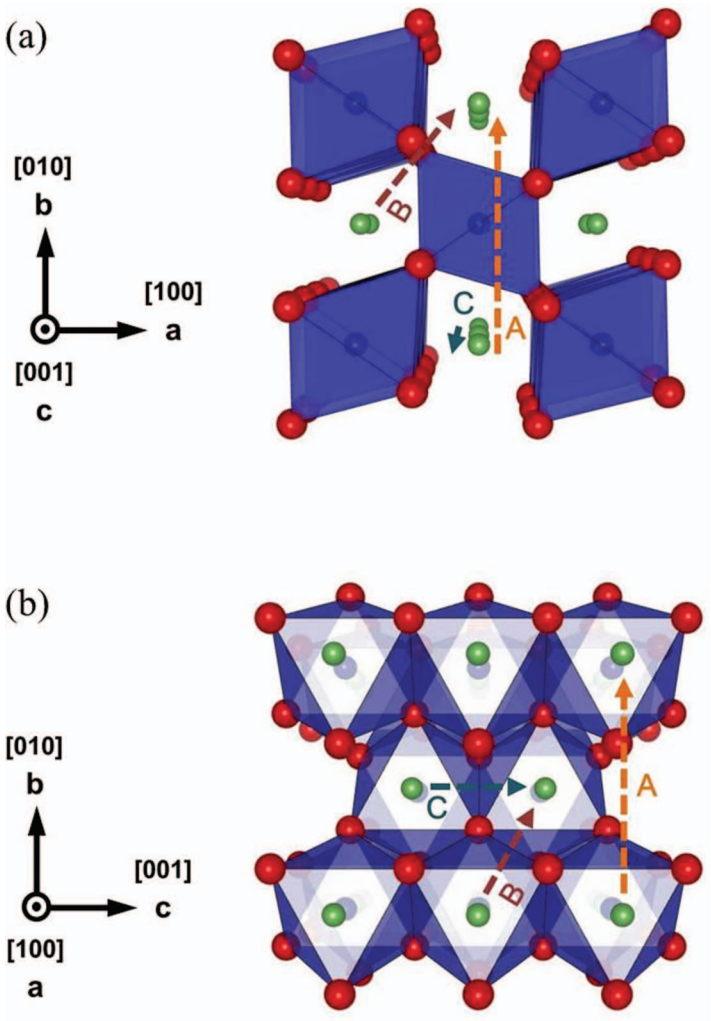

FIG. 2. Possible Li migration pathways in (a) *a* axis view and (b) *c* axis view. Green spheres are Li ions, blue octahedrons with red spheres at corners are RuO_6. Path A represents jump of Li along the *b* direction through Ru-O octahedrons, Path B represents movement of Li to the next channel, and path C corresponds to Li movement along a channel parallel to the *c* direction.

[111] direction (Path B), and movement in the open channel along the c-axis in the [001] direction (Path C).

Stable positions of Li ions corresponding to local energy minima are identified through atomic relaxation after a vacancy is introduced at the original Li site. For the Li-rich phase ($Li_{15}Ru_{16}O_{32}$), the overall structure remains similar to the perfect structure of $LiRuO_2$. Specifically, the energy minima of Li ions are located at the octahedral sites. The migration energy barrier is defined as the energy difference between the local minima and the saddle point corresponding to the highest energy level along a Li migration pathway. For path A, the saddle point occurs at the edge of the edge-sharing octahedrons and Li ions with low levels of energy are not expected to pass through it. The calculations show that the energy barrier is high, at 8.77 eV, suggesting that path A is unlikely to be a feasible pathway. The saddle point along path B is located where Li passes through a gap between two corner-sharing and one edge-sharing RuO_6 octahedrons. Here, Li has a short bond length of 1.71 Å with three neighboring O atoms and a high migration energy barrier of 2.41 eV. Path C has the lowest migration energy barrier of 0.56 eV. The undistorted, straight migration trajectory is along the *c*-channel and Li forms a 2-fold coordinated LiO_6 octahedron with bond lengths of 1.77 Å and 2.50 Å at the saddle point. Table III lists the nearest-neighbor Li-Ru and Li-O distances.

TABLE III. Nearest-neighbor distances in RuO_2. The number of bonds is in the parentheses.

	Li-rich		Li-poor	
	$d_{Li\text{-}O}$ (Å)	$d_{Li\text{-}Ru}$ (Å)	$d_{Li\text{-}O}$ (Å)	$d_{Li\text{-}Ru}$ (Å)
Energy minimum points	2.10 (×4)	2.86 (×4)	1.85 (×4)	2.49 (×4)
	2.08 (×2)	2.56 (×2)		
Saddle points	2.49 (×4)	2.90 (×4)	2.22 (×4)	2.79 (×4)
	1.77 (×2)	2.54 (×2)	1.80 (×2)	2.40 (×2)

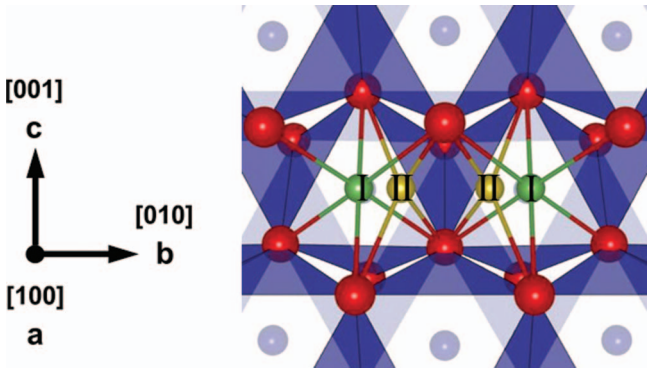

FIG. 3. Stable Li positions at local energy minima in the host structure. I and II denote the positions corresponding to the Li-rich and Li-poor regions, respectively.

As the probability of ion hopping decreases exponentially with the migration energy barrier, the significantly higher migration energy barriers for paths A and B compared with the energy barrier of path C shows that Li diffusion is one-dimensional, and channel C is the only viable migration path. The energy barrier calculated here is in excellent agreement with the result of a galvanostatic study (0.52 eV) conducted by Dalard *et al.*[9]

C. Migration energy barriers in Li-poor phase

Similar to the Li-rich phase, the three possible pathways for Li migration in the Li-poor phase are also studied. The pathways are similarly defined as those in the Li-rich phase (see Figure 2). A noticeable difference in the Li-poor phase is that the local energy minimum points of intercalated Li are not located at the same sites as in the Li-rich phase. The minimum is at a tetrahedral site which deviates from the octahedral site by 0.75 Å (0.12c) in the *c* direction, as shown in Figure 3. As a result, Li forms a LiO_4 tetrahedron with a shorter Li-O distance of 1.85 Å in the relaxed structure, instead of forming a LiO_6 octahedron seen in the Li-rich phase. This change leads to a reduction in the migration distance along all pathways. Here, the stable Li placement in the rutile host corresponds to the Wyckoff position of 8(h) with (0, 1/2, z = 0.257) in the 136 ($P4_{2/mnm}$) space group.

The NEB calculations show that the energy barriers are 7.47 eV, 1.75 eV, and 0.16 eV for path A, path B, and path C, respectively. Path B has a similar trajectory, except that the initial and end points are located differently as described above. Li ions move through saddle points located within RuO_6 octahedrons along a helical trajectory depicted in Figure 4. The significantly lower migration barrier for path C also confirms that the one-dimensional diffusion along the *c* direction is the actual migration path in the Li-poor phase. The saddle point is located at the octahedral site, as in the Li-rich phase. The migration distance of Li is 1.62 Å, shorter than the distance of 2.78 Å in the Li-rich phase. Since the number of saddle points and the local minima per unit cell in the Li-poor phase are twice those in the Li-rich phase (see Figure 3), the migration period of Li in the Li-poor phase is one half that in the Li-rich phase, i.e. 0.5c in Li-poor phase, 1c in Li-rich phase (c is the lattice parameter along the [001] direction). This difference causes the migration distance in the

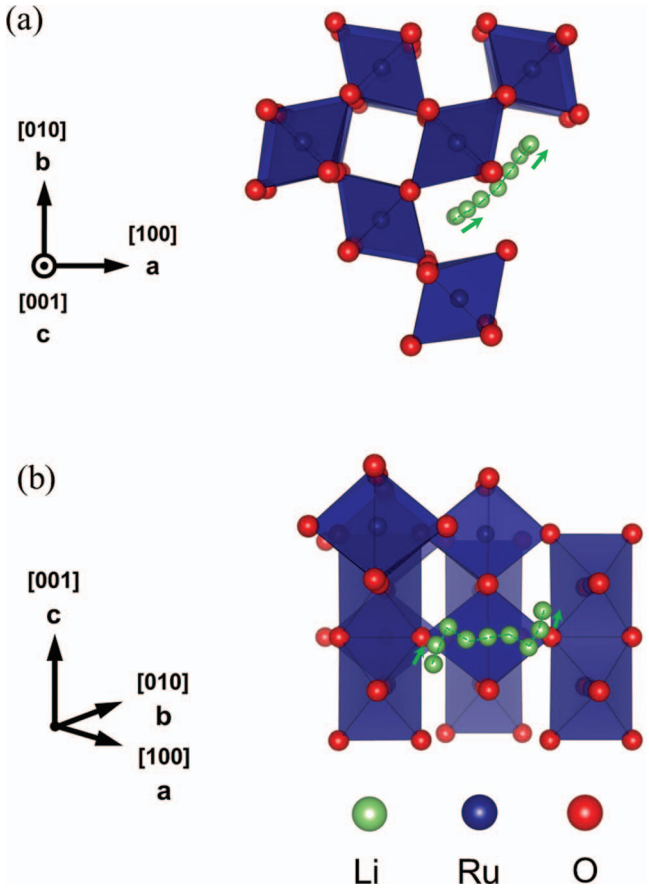

FIG. 4. Trajectory of Li migration for path B.

Li-poor phase to be shorter, even though the Li-poor phase has a larger lattice parameter in the *c* direction.

The Li-O bond lengths and Li-Ru interatomic distances are listed in Table III. At the saddle points for both phases, the lengths of two of the six Li−O bonds become shorter compared with the lengths of the other four bonds, making the LiO_6 octahedra more distorted compared with the respective initial states. The lower energy barrier indicates that the diffusion of Li ions occurs more easily in the Li-poor state. The energy profiles along migration path C in the Li-rich and Li-poor phases are illustrated in Figure 5. At the saddle point, the Li ion experiences the highest Coulombic repulsion due to Ru cations located perpendicular to the migration path. As discussed earlier, a partial covalent characteristic of bonding exists between the Ru and O compounds. When a charge is introduced with the Li^+ ion in the electrode structure, the charge is partially donated to Ru cations and O anions and the covalent characteristic remains. In contrast, the repulsion between Li cations along the *c* direction is insufficiently screened. Therefore, a Li ion at the saddle point in the Li-rich phase experiences a larger level of electrostatic repulsion from other Li ions along the *c*-channel. This effect induces a higher Li migration energy barrier in the Li-rich phase than in the Li-poor phase.

D. Comparison with TiO_2

Another material having the same rutile structure is TiO_2. It has been extensively studied and has attracted attention for a long time. In spite of its abundance and low cost, rutile TiO_2 has encountered difficulty in commercialization due to its limitation on Li insertion at room temperature. DFT studies revealed that it can be explained by a combination of anisotropic diffusion in the *c*-channel

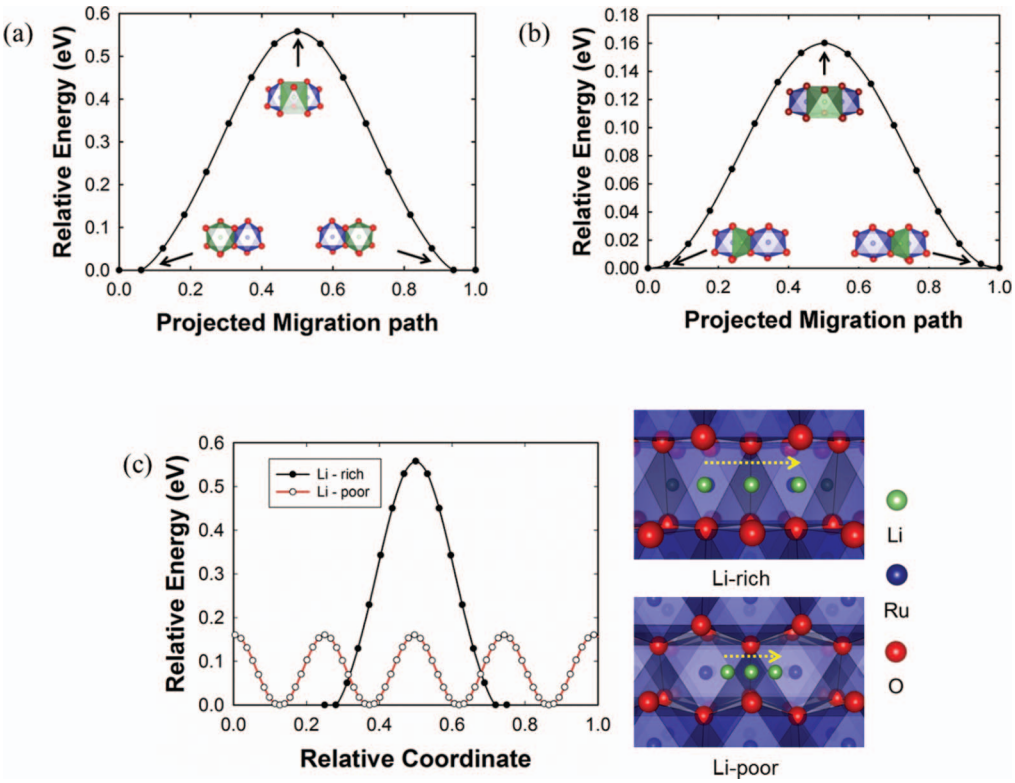

FIG. 5. Energy profiles along path C. (a) Li-rich phase, Li ions move from the local minimum position forming Li-O octahedrons to the symmetric nearest neighbor position. (b) Li-poor phase, Li ions move from the deviated tetrahedron position to the next nearest neighbor position. (c) Li-rich phase (black) and Li-poor phase (red) along the c-direction. The relative coordinate indicates relative position projected in the [0 0 1] direction along the *c*-axis. 2c (size of the supercells along the [0 0 1] direction) scales to 1.0. Li migration trajectories for Li-rich phase and Li-poor phase are depicted. Yellow arrows indicate the trajectories from a local minimum to the nearest minimum.

and favorable energetic ordering of Li ions along *ab* planes at low Li concentrations.[23–25] Migration energy barrier calculations in the literature have focused on diffusion of Li in the $Li_{0.5}TiO_2$ structure. We have extended the analysis of Li diffusion into Li-rich ($Li_{15}Ti_{16}O_{32}$) and Li-poor ($Li_1Ti_{16}O_{32}$) cases using identical approaches we used for RuO_2. Perfect unit cell structures of TiO_2 and $LiTiO_2$ are fully relaxed to obtain optimized lattice parameters of a = b = 4.656 Å and c = 2.971 Å for TiO_2, and a = 5.069 Å, b = 5.008 Å, and c = 2.846 Å for $LiTiO_2$. The NEB calculations are performed in supercells consisting of 2a × 2b × 2c unit cells which contain 16 formula units to reduce interactions between images due to the periodic boundary conditions used. Structural parameters of perfect TiO_2 and $LiTiO_2$ are used in the models of the Li-poor phase and the Li-rich phase, respectively. The migration barriers are calculated to be 0.43 eV and 0.03 eV in the Li-rich and Li-poor phases, respectively. A very low energy barrier for Li diffusion in the Li-poor phase is consistent with reported the migration barrier of 0.04 eV in relaxed the structure of $Li_{0.5}TiO_2$.[24] Calculated atomic distances, energy barriers, and migration distances are listed in Table IV. The energy profiles are shown in Figure 6. The migration distance is shorter in the Li-poor phase, as in RuO_2. Nevertheless, the local minimum points are located in octahedral sites, and the saddle point is located in tetrahedral sites, opposite to what is seen in RuO_2. In other words, the positions of the local minima in RuO_2 are the positions of saddle points in TiO_2, and vice versa.

As described earlier, the low Li diffusivity in *ab* planes prevents Li to be favorably ordered in TiO_2.[23,25] In contrast, Li diffusion can occur easily in RuO_2 at room temperature. In order to compute the energetically favorable site of the added Li, we compared the total energy changes due to the intercalation of an additional Li in the Li-poor phases of RuO_2 and TiO_2. The energy changes are computed by placing one Li atom at the nearest minimum points along the *a*, *b*, and *c* directions

TABLE IV. Nearest-neighbor distances, migration distances, and migration energies in TiO_2. The number of bonds is in the parentheses.

	Li–poor		Li–rich	
	$d_{Li\text{-}O}$ (Å)	$d_{Li\text{-}Ti}$ (Å)	$d_{Li\text{-}O}$ (Å)	$d_{Li\text{-}Ti}$ (Å)
Energy minimum points	1.82 (×2)	2.54 (×2)	1.99 (×2)	2.55 (×2)
	2.11 (×4)	2.81 (×4)	2.16 (×4)	2.86 (×4)
Saddle points	1.84 (×4)	2.62 (×4)	1.79 (×2)	2.58 (×2)
			2.40 (×4)	2.86 (×4)
Migration distance (Å)	1.49		2.85	
Migration energy (eV)	0.03		0.43	

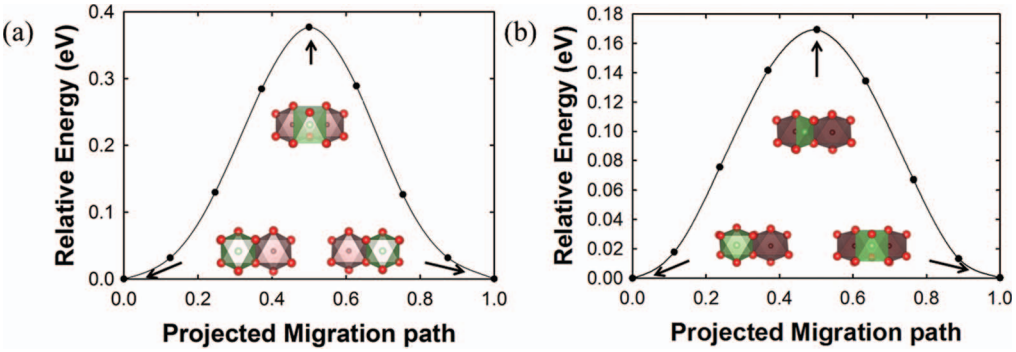

FIG. 6. Energy profiles along path C of TiO_2. (a) Li-rich phase. (b) Li-poor phase.

in the relaxed Li-poor structure. It is found that the energy is higher when Li ions are arranged along the *c* direction than when they are arranged along the *b* or *a* direction. The corresponding energy difference is 0.02 eV and 0.23 eV in RuO_2 and TiO_2, respectively. The energy difference in RuO_2 is much lower than that in TiO_2. As a result, the negative effect of low diffusivity in *ab* planes on the migration of Li along *c* channels in RuO_2 is not as pronounced as in TiO_2. Therefore, unlike in TiO_2, Li can be inserted into RuO_2 at low concentrations and relatively low temperatures.

E. Diffusivity

The diffusivity can be calculated from the energy barriers along migration paths using the transition state theory. Specifically, for a system with non-interacting particles (either interstitials Li or vacancies of low concentrations) – which is the case for the phases considered in this study, the diffusivity can be expressed as[26]

$$D = \Gamma d^2, \tag{1}$$

where Γ is the rate of hopping to a neighboring site and d is the migration distance. This hopping rate can be expressed as

$$\Gamma = \upsilon^* e^{-\Delta E/k_b T}, \tag{2}$$

where ΔE is the energy barrier, T is the absolute temperature, k_b is Boltzmann's constant, and υ^* is the effective frequency associated with the vibration of the defect, which has usually been assumed to be a constant of 1.0×10^{13} Hz or 1.0×10^{12} Hz in previous DFT calculations of diffusivities.[27–31] In this study, we compute the effective frequency to allow a more accurate comparison of the diffusional behavior at different Li concentrations. Previous studies of Li diffusion in carbon-based electrode materials in different conditions were conducted by direct calculation of phonon frequencies and were in good agreement with experiments.[32,33] According to Vineyard,[34] for a system containing N

TABLE V. Migration energy barriers, effective frequencies for Li migration, diffusivities from calculations and experiments, and Li migration distances between stable points of RuO_2 host.

	Li - poor	Li - rich	Experiments
Migration energy (eV)	0.16	0.56	0.52[9]
Effective frequency (Hz)	5.5×10^{13}	6.7×10^{12}	
Diffusivity (cm^2/s)	1.0×10^{-5}	1.0×10^{-12}	1.6×10^{-11} (80 °C)[8]
			2.0×10^{-11} (25 °C)[8]
Migration distance (Å)	1.57	2.79	

atoms υ^* can be evaluated as

$$\upsilon^* = \frac{\prod_{i=1}^{3N} \upsilon^I{}_i}{\prod_{j=1}^{3N-1} \upsilon^S{}_j}, \tag{3}$$

where υ^I and υ^S are the normal mode vibrational frequencies at the initial and saddle points, respectively. Using force constants obtained from DFPT (Density functional perturbation theory) calculations, we have evaluated the normal phonon frequencies. The phonon calculations are performed using the PHONOPY code.[35–37] For this purpose, equation (1) is rewritten as

$$D = \frac{\prod_{i=1}^{3N} \upsilon^I{}_i}{\prod_{j=1}^{3N-1} \upsilon^S{}_j} d^2 e^{-\Delta E/k_b T}. \tag{4}$$

This expression involves temperature and quantities obtained from *ab initio* calculations. At the saddle point, the number of degrees of freedom for phonon frequencies is one less than that at the initial point. The effective frequencies are found to be 6.7×10^{12} Hz for the Li-rich phase and 5.5×10^{13} Hz for the Li-poor phase. The higher effective frequency for the Li-poor phase leads to faster Li diffusion and reflects the lower migration energy barrier compared with the Li-rich phase. For instance, at room temperature (300 K), the diffusivities are found to be 1.0×10^{-12} cm^2/s for the Li-rich phase and 1.0×10^{-5} cm^2/s for the Li-poor phase. Table V lists migration energy barriers, effective frequencies for Li migration, diffusivities from calculations and experiments, and Li migration distances between stable points of RuO_2 host.

Experimental measurements conducted at 25 $\sim$ 80 °C show Li diffusivities of 0.9×10^{-12} -2×10^{-11} cm^2/s,[8,9] which lie within the range of our computational results for the Li-poor and Li-rich phases. Recently, Delmer *et al.*[10] measured the Li diffusivity in RuO_2 nanoparticles using the GITT (Galvanostatic intermittent titration technique) experiment and reported a maximum value of around 9×10^{-11} cm^2/s in low Li-concentration regions. In all the reported experiments, a rapid voltage drop is observed at the beginning of the discharging process. Since the diffusivity is proportional to square of dE/dx (E is the voltage and x is that in Li_xRuO_2), a significant voltage drop indicates faster diffusion at low Li concentrations. It is observed that the diffusivity is lower by four orders of magnitude (10^4 times) at the beginning of the discharge process.[10] As the compositions of the structures in our simulations vary from those from experiments reported in the literature, direct validations of properties are challenging. Specifically, the experimentally observable structure of dilute regions in cathodes may not have exactly the same composition as our Li-poor phase, but rather have combined features of ideal structures of Li-poor and Li-rich phases as we have considered. Nevertheless, our results account for the overall qualitative features during charging/discharging observed in experiments. Although our theoretical value for the diffusivity of the Li-poor phase is higher than the experimental value, it is qualitatively consistent with the trend of slowing diffusion as Li insertion progresses.

IV. CONCLUSION

The diffusional behavior of Li ions in rutile structure RuO_2 in both Li-rich and Li-poor phases is investigated using DFT-based first-principles calculations. The energy barriers through likely migration pathways for the Li-rich and Li-poor phases are quantified to be 0.56 eV and 0.16 eV, respectively. The anisotropic one-dimensional diffusion of Li along the *c*-axis in the [001] direction of rutile RuO_2 is found to have the lowest migration energy barrier compared with other possible pathways. A comparison with TiO_2 rutile host is made. It is found that the energetically favored ordering of Li in RuO_2 along the *c* direction enables Li insertion into RuO_2 at ambient temperature, an attribute not observed in TiO_2.

The diffusivities of the Li-rich and Li-poor phases are calculated to be 1.0×10^{-12} cm^2/s and 1.0×10^{-5} cm^2/s at room temperature, respectively. The diffusivity of the Li-rich phase is consistent with experimental measurements. In addition, our result accounts for the diffusional behavior difference associated with Li concentration differences. A much lower migration energy barrier and a higher effective frequency are found for the Li-poor phase relative to the Li-rich phase. It is this difference in energy barriers and effective frequencies between the two phases that leads to the drastically lower diffusivity of the Li-rich phase compared with the Li-poor phase. The analysis suggests that taking advantage of fast anisotropic one-dimensional channels for Li transport can be an effective mechanism for the design of positive electrode materials for lithium ion batteries.

ACKNOWLEDGMENT

Support by the National Research Foundation of Korea through WCU_Grant No. R31-2009-000-10083-0 is gratefully acknowledged.

[1] P. Balaya, H. Li, L. Kienle, and J. Maier, Advanced Functional Materials **13**(8), 621–625 (2003).
[2] T. Ohzuku, K. Sawai, and T. Hirai, Journal of the Electrochemical Society **137**, 3004 (1990).
[3] E. Bekaert, P. Balaya, S. Murugavel, J. Maier, and M. Meéneétrier, Chemistry of materials **21**(5), 856–861 (2009).
[4] H. X. Ji, X. L. Wu, L. Z. Fan, C. Krien, I. Fiering, Y. G. Guo, Y. Mei, and O. G. Schmidt, Advanced Materials **22**(41), 4591–4595 (2010).
[5] Y. S. Hu, Y. G. Guo, R. Dominko, M. Gaberscek, J. Jamnik, and J. Maier, Advanced Materials **19**(15), 1963–1966 (2007).
[6] F. Zhang, S. Passerini, B. B. Owens, and W. H. Smyrl, Electrochemical and Solid-State Letters **4**, A221 (2001).
[7] J. Liu and A. Manthiram, J. Mater. Chem. **20**(19), 3961–3967 (2010).
[8] M. Armand, F. Dalard, D. Deroo, and C. Mouliom, Solid State Ionics **15**(3), 205–210 (1985).
[9] P. Dalard, D. Deroo, D. Foscallo, and C. Mouliom, Solid State Ionics **15**(2), 91–94 (1985).
[10] O. Delmer, "Max Planck Institute for Solid State Research," Stuttgart (2010).
[11] W. Ryden, A. Lawson, and C. C. Sartain, Physical Review B **1**, 1494–1500 (1970).
[12] G. Kresse and J. Furthmüller, Physical Review B **54**(16), 11169 (1996).
[13] G. Kresse and D. Joubert, Physical Review B **59**(3), 1758 (1999).
[14] P. E. Blöchl, Physical Review B **50**(24), 17953 (1994).
[15] J. P. Perdew, J. Chevary, S. Vosko, K. A. Jackson, M. R. Pederson, D. Singh, and C. Fiolhais, Physical Review B **46**(11), 6671 (1992).
[16] G. Henkelman, B. P. Uberuaga, and H. Jónsson, The Journal of Chemical Physics **113**, 9901 (2000).
[17] H. Jonsson, G. Mills, and K. W. Jacobsen, Nudged Elastic Band Method for Finding Minimum Energy Paths of Transitions, in *Classical and Quantum Dynamics in Condensed Phase Simulations* (World Scientific, Singapore, 1998).
[18] M. Johannes, A. Stux, and K. Swider-Lyons, Physical Review B **77**(7), 075124 (2008).
[19] I. J. Davidson and J. Greedan, Journal of Solid State Chemistry **51**(1), 104–117 (1984).
[20] D. Murphy, F. Di Salvo, J. Carides, and J. Waszczak, Materials Research Bulletin **13**(12), 1395–1402 (1978).
[21] G. Henkelman, A. Arnaldsson, and H. Jónsson, Computational Materials Science **36**(3), 354–360 (2006).
[22] E. Sanville, S. D. Kenny, R. Smith, and G. Henkelman, Journal of Computational Chemistry **28**(5), 899–908 (2007).
[23] M. V. Koudriachova, N. M. Harrison, and S. W. de Leeuw, Physical Review Letters **86**(7), 1275–1278 (2001).
[24] M. V. Koudriachova, N. M. Harrison, and S. W. de Leeuw, Solid State Ionics **157**(1), 35–38 (2003).
[25] M. V. Koudriachova, N. M. Harrison, and S. W. de Leeuw, Physical Review B **65**(23), 235423 (2002).
[26] N. Peterson, Journal of Nuclear Materials **69**, 3–37 (1978).
[27] W. Frank, U. Breier, C. Elsässer, and M. Fähnle, Physical Review Letters **77**(3), 518–521 (1996).
[28] F. Montalenti, D. Migas, F. Gamba, and L. Miglio, Physical Review B **70**(24), 245315 (2004).
[29] D. Morgan, A. Van der Ven, and G. Ceder, Electrochemical and Solid-State Letters **7**, A30 (2004).
[30] T. Mueller, G. Hautier, A. Jain, and G. Ceder, Chemistry of materials **23**(17), 3854–3862 (2011).
[31] K. Kang, D. Morgan, and G. Ceder, Physical Review B **79**(1), 014305 (2009).

[32] K. Toyoura, Y. Koyama, A. Kuwabara, F. Oba, and I. Tanaka, Physical Review B **78**(21), 214303 (2008).
[33] K. Toyoura, Y. Koyama, A. Kuwabara, and I. Tanaka, The Journal of Physical Chemistry C **114**(5), 2375–2379 (2010).
[34] G. H. Vineyard, Journal of Physics and Chemistry of Solids **3**(1–2), 121–127 (1957).
[35] A. Togo, L. Chaput, I. Tanaka, and G. Hug, Physical Review B **81**(17), 174301 (2010).
[36] A. Togo, F. Oba, and I. Tanaka, Physical Review B **78**(13), 134106 (2008).
[37] A. Togo, Phonopy http://phonopy.sourceforge.net/.